Journal of Power Sources 204 (2012) 230–235

Contents lists available at SciVerse ScienceDirect

Journal of Power Sources

journal homepage: www.elsevier.com/locate/jpowsour

A novel mesoporous carbon with straight tunnel-like pore structure for high rate electrochemical capacitors

Wenfeng Zhang[a,b], Zheng-Hong Huang[a], Gaoping Cao[b], Feiyu Kang[a,*], Yusheng Yang[b]

[a] State Key Laboratory of New Ceramics and Fine Processing, Department of Materials Science and Engineering, Tsinghua University, Beijing 100084, China
[b] Research Institute of Chemical Defense, Beijing 100191, China

ARTICLE INFO

Article history:
Received 25 September 2011
Received in revised form
26 December 2011
Accepted 27 December 2011
Available online 5 January 2012

Keywords:
Mesoporous carbon
One dimension structure
Template
Electrochemical capacitors

ABSTRACT

Mesoporous carbons are prepared from a mixture of the soluble starch with needle-like nano-sized $Mg(OH)_2$ particles. The samples structures are characterized by TEM, nitrogen adsorption at 77 K and XRD. The electrochemical performance for electrochemical capacitors is evaluated in a 6 M KOH aqueous solution. The resultant carbons show a disordered pore structure with interweaving straight nano-tunnels that resembled the shape of the template, and possess a high surface area more than 1000 $m^2 g^{-1}$ and a large pore volume. The special one dimensional morphology of templates cause a graphitization effect on the carbon in partial region, different from catalytic graphitization mechanism of transition metal particles. Due to those characteristics, the samples exhibit good electrochemical performances used for electrochemical capacitors electrode, especially excellent power capability. The sample carbonized at 950 °C for 6 h retain a capacitance of 126 F g^{-1} even at a high current density of 40 A g^{-1}.

1. Introduction

Electrochemical capacitors (ECs) have been becoming attractive energy storage systems, particularly for applications involving high power requirements [1]. Porous carbon materials, one of the most important candidates for ECs electrode materials, have been widely used in practical application. Some crucial characteristics of porous carbons, such as a large surface area for charge accumulation, an appropriate pore structure for electrolyte wetting and rapid ionic motion, and high electrical conductivity, are highly desirable to exhibit good electrochemical performances [2,3]. It was proved that extremely narrow pore (<1 nm) is optimal to increasing energy density [4,5]. But for power applications, except few sorts of micropores with special morphology such as those are three-dimensionally arrayed and mutually connected [6], increasing the pore size to mesoporous (>2 nm) might be more beneficial.

Over the last decade, there have been significant advances in the synthesis of mesoporous carbon materials [7,8]. One efficient method to obtain mesoporous carbons is using template carbonization route, which allows the preparation of carbon materials with controlled architecture and relatively narrow pore size distribution. Since the synthesis of mesoporous M41S silica materials was reported by Mobil Corporation researchers in 1992, mesoporous silicas with interconnected pore structures have been successfully used as templates for the synthesis of mesoporous carbon materials. Various mesoporous carbon materials with different pore structures were synthesized using a variety of different mesoporous silica templates, such as MCM-48, MCM-41, HMS, SBA-15, and MSU-X [9,10]. However, the procedure employed to synthesize mesoporous carbons using meso-structured silica templates is rather complicated and time consuming, which limits the application of ordered mesoporous carbons. More recently, significant progress has been achieved on the direct synthesis of ordered mesoporous carbon materials by the self-assembly of organic–organic species as so-called soft templating [11–17]. Mesoporous carbons with controlled pore structures can be obtained more flexibly with fewer synthesis steps. Currently, there exist only a few successful experiments that fabricate porous carbon via soft templating methods. Mesoporous carbons created through this method possessed relatively lower surface areas and smaller pore volumes, which cannot satisfy the demands of ECs electrode applications. In comparison, an attractive method for preparing porous carbons with disordered pore structure using metal oxides as template was developed by Inagaki et al. [18–21]. Thermoplastic precursors mixed with MgO itself or precursors of MgO, such as Mg acetate, Mg citrate and Mg gluconate, were carbonized at high temperatures in an inert atmosphere. After carbonization, the MgO was easily extracted using diluted sulfuric acid and then the formed carbons were isolated. The pore size was governed by the size of MgO particles. These carbons obtained by different mixing methods possessed a large amount of mesopores and high surface areas.

* Corresponding author. Fax: +86 10 62771160.
E-mail address: fykang@tsinghua.edu.cn (F. Kang).

0378-7753/$ – see front matter © 2012 Elsevier B.V. All rights reserved.
doi:10.1016/j.jpowsour.2011.12.054

In the present study, a novel mesoporous carbon with straight tunnel-like pore structure was prepared from a mixture of the soluble starch with needle-like nano-sized $Mg(OH)_2$ particles. The structures of the resultant mesoporous carbons were characterized, and the electrochemical performance of the sample for ECs electrode material was investigated.

2. Experimental

The needle-like nano-sized $Mg(OH)_2$ was prepared by the surfactant-mediated solution procedure outlined in the literature [22]. The typical synthetic process of porous carbons proceeds as follows: 10.0 g $Mg(OH)_2$ was dispersed in 40 mL deionized water for 1 h with ultrasonic stirring. 10.0 g soluble starch (30% aqueous solution) was then added into the $Mg(OH)_2$ suspension, and mixed 1 h with ultrasonic stirring. The mixture was vacuum-dried at 50 °C for 12 h. Afterwards, the dried mixture was carbonized above 750 °C. The derived products were immersed in 2 mol L^{-1} sulfuric acid to dissolve the MgO, and then washed with deionized water. The resultant porous carbon was denoted as SMC-55-X-Y (X and Y denotes carbonization temperature and duration, respectively. "55" denotes the ratio between starch and $Mg(OH)_2$). For a comparison, the soluble starch without $Mg(OH)_2$ was also carbonized at different temperatures, and the derived carbons were denoted as SC-X-Y (X and Y mean as above).

TEM images were observed on a JEM2010 electron microscope operating at 200 kV. N_2 sorption isotherms were measured using a Quantachrome Autosorb-1 Adsorption Apparatus at 77 K. XRD patterns were obtained on a D8 Advance Diffractometer (Bruker AXS) with a Cu Kα source.

Electrochemical measurements were carried out in a 6 mol L^{-1} KOH aqueous electrolyte at room temperature, using a three-electrode cell with a Hg/HgO reference electrode and a platinum coil counter electrode. The testing electrodes were prepared by mixing porous carbon powders, carbon black and polytetrafluorethylene (PTFE) together at a mass ratio of 85:10:5, and rolling the resulting mixture into a film about 0.18 mm in thickness. The film was cut into 1 cm by 1 cm pieces and covered on plain nickel foam (current collector) with a corresponding shape before being pressed together at 0.6 MPa. The electrochemical characteristics of samples were determined by galvanostatic charge/discharge, cyclic voltammetry (CV), and electrochemical impedance spectroscopy (EIS). Galvanostatic charge/discharge measurements were carried out by an Arbin-BT2000 (Arbin Instruments) test station at different current densities from 0.5 A g^{-1} to 40 A g^{-1}, with the potential window from −0.8 to 0.0 V (vs. Hg/HgO). A Solartron Instrument Model 1287 electrochemical interface was used for CV and EIS measurements. EIS measurements were conducted in the constant potential mode by sweeping the frequencies from 20 kHz to 0.1 Hz range with an AC-amplitude of 10 mV.

3. Results and discussion

3.1. Structures characterization

In order to study the effect of the one-dimensional template on the pores of carbon, a sample denoted as SMC-51-950-1 obtained from the mixture with a low template quantity was characterized by TEM. The dispersed $Mg(OH)_2$ nanoparticles display needle-like morphologies with diameters of 4–10 nm and lengths of 50–100 nm (Fig. 1a). $Mg(OH)_2$ can transform into MgO at temperatures of 300–400 °C, while the needle-like morphological feature remain [23]. It is interesting to note that the pores of mesoporous carbon resemble the shape of needle-like nano-sized particles,

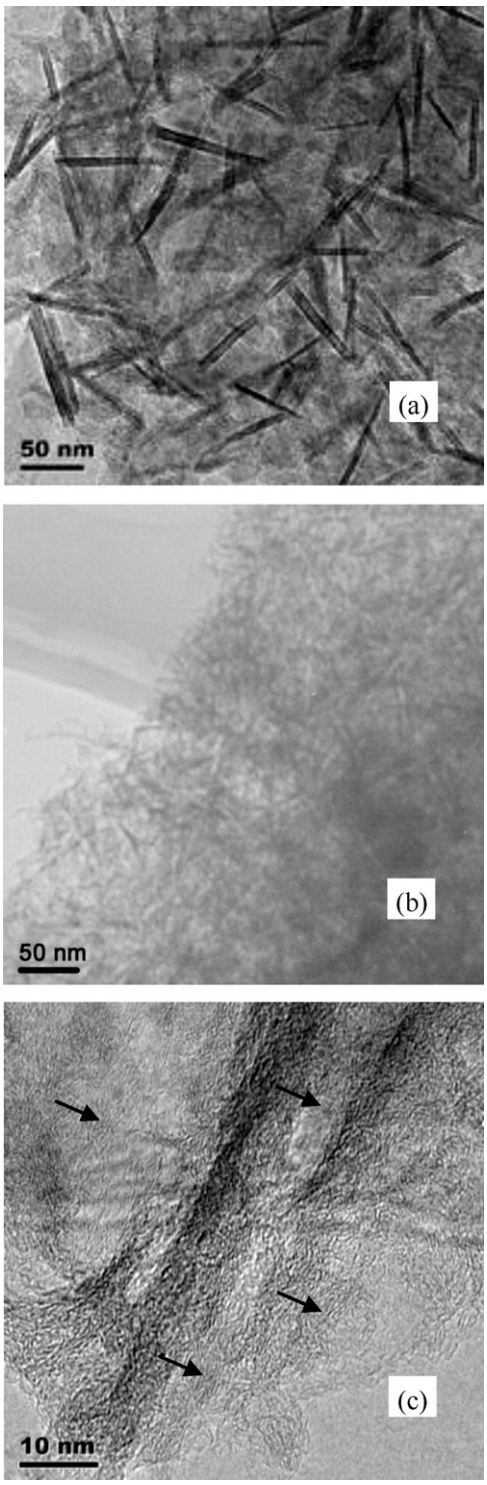

Fig. 1. TEM images of (a) needle-like nano-sized $Mg(OH)_2$ and (b) SMC-51-950-1 (the proportion between soluble starch and $Mg(OH)_2$ was 5:1, carbonized at 950 °C for 1 h); and (c) HRTEM image of SMC-51-950-1.

and exhibits a disordered porous structure with interweaving 1D straight nano-tunnels (Fig. 1b and c).

Fig. 2 shows the nitrogen adsorption–desorption isotherms at 77 K of SC-850-3, SMC-55-750-3, SMC-55-950-3 and SMC-55-950-6. It can be seen that, the amount adsorbed of SC-850-3 is so small, suggesting few pores in the sample. While for carbons synthesized with template, after a large micropore volume filling at lower pressures, the amount adsorbed increases gradually as the relative

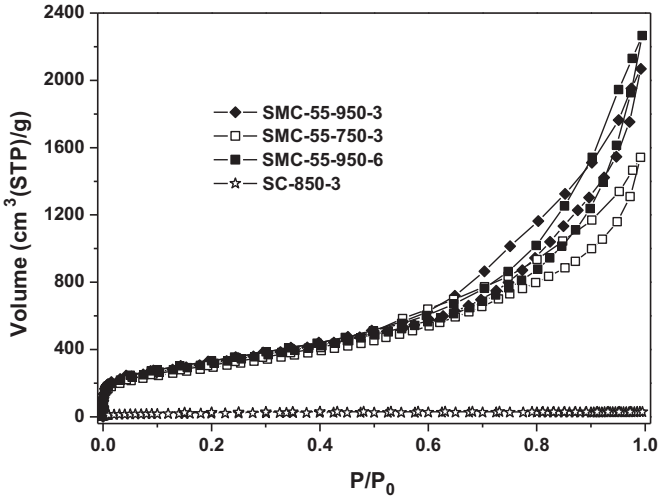

Fig. 2. Isotherms of porous carbons measured by nitrogen adsorption at 77 K.

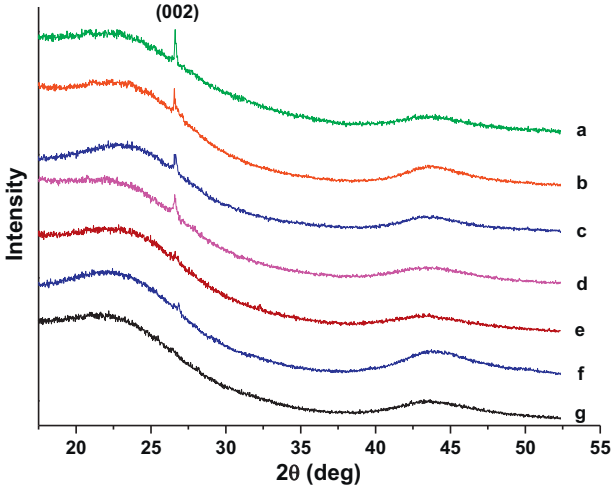

Fig. 4. XRD patterns of the resulting carbons.

pressure increases. Close to the saturation vapor pressure, the amount adsorbed rise very steeply, while the adsorption isotherm do not level off, which means unrestricted multilayer formation process of macropores. In addition, the adsorption and desorption branches of the isotherm do not coincide, and a pronounced adsorption–desorption hysteresis can be seen. Therefore, the nitrogen isotherm may be classified as a combination of type II and type IV adsorptions [24]. The pronounced hysteresis loop suggests a higher amount of mesopores. The pore-size distributions calculated on the basis of the desorption branch of the isotherm are shown in Fig. 3. A relatively narrow pore-size distribution with a maximum of mesopores small than 10 nm are detected, corresponding to the diameter size of the $Mg(OH)_2$ template. This indicates that the pores in the carbon were formed by removing template mainly. Increasing the carbonization temperature, the size of those mesopores increases, and the pore volumes (at $p/p_0 = 0.99$) also increase greatly, from 2.39 $cm^3\,g^{-1}$ of SMC-55-750-3 to 3.21 $cm^3\,g^{-1}$ of SMC-55-950-3 and 3.51 $cm^3\,g^{-1}$ of SMC-55-950-6, which can be ascribed to the collapse of pores wall at higher carbonization temperature. However, the effect of carbonization temperature on the BET surface area is not so great. The surface area of SMC-55-750-3 reaches 1014 $m^2\,g^{-1}$, while that of SMC-55-950-3 and SMC-55-950-6 are 1070 $m^2\,g^{-1}$ and 1060 $m^2\,g^{-1}$, respectively.

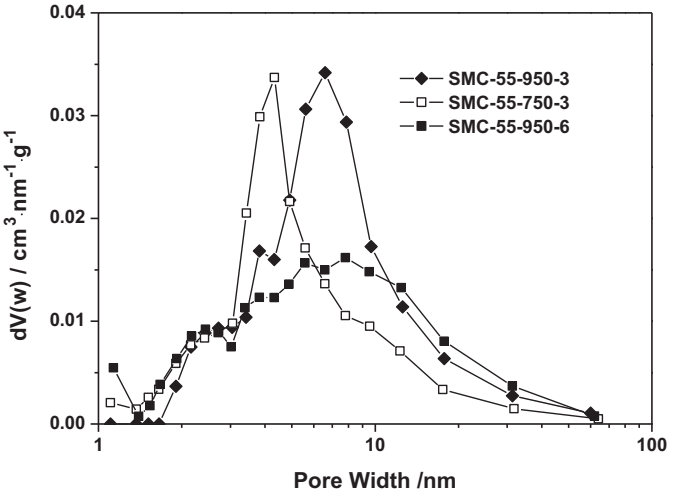

Fig. 3. The pore distribution determined by BJH method.

Fig. 4 shows the XRD patterns of the resulting carbons. All of the resultant carbons exhibit an amorphous structure characteristic. However, it is interesting to note that there are obvious peaks at $2\theta = 26.6^\circ$ appeared for the samples obtained in the presence of needle-like nano-sized $Mg(OH)_2$ above 850 °C. To identify the certain components of the carbon, the ash contents of the samples were tested by heating them up to 800 °C for 1 h in air in the muffle furnace. It was found that the ash contents of SMC-55-850-3 and SMC-55-950-6, which was mainly MgO unremoved, were 0.04% and 0.07%, respectively. Such a small impurity content is not enough to cause any peak in XRD analysis. So the peaks of XRD patterns in Fig. 4 can be assigned to the (0 0 2) diffraction of the graphitic framework. Those diffraction peaks become stronger when the heat treatment temperature increase,

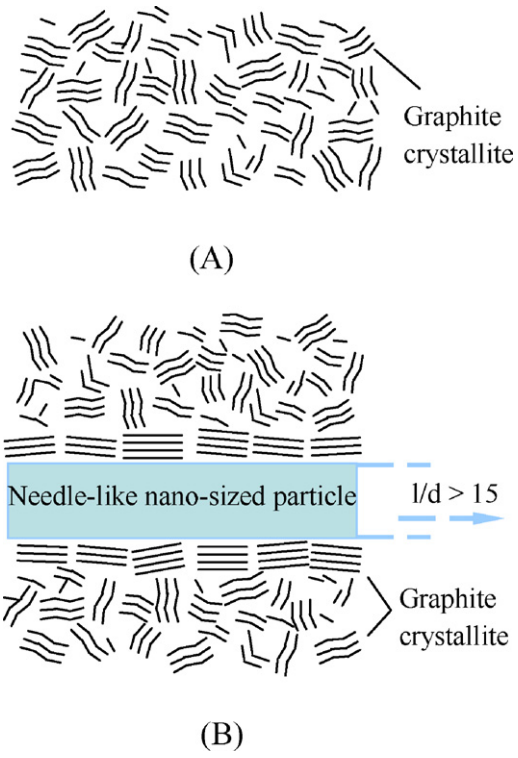

Fig. 5. Schematic diagram of the formation mechanism of graphite-like structure in partial region with one dimensional nano-sized particle template.

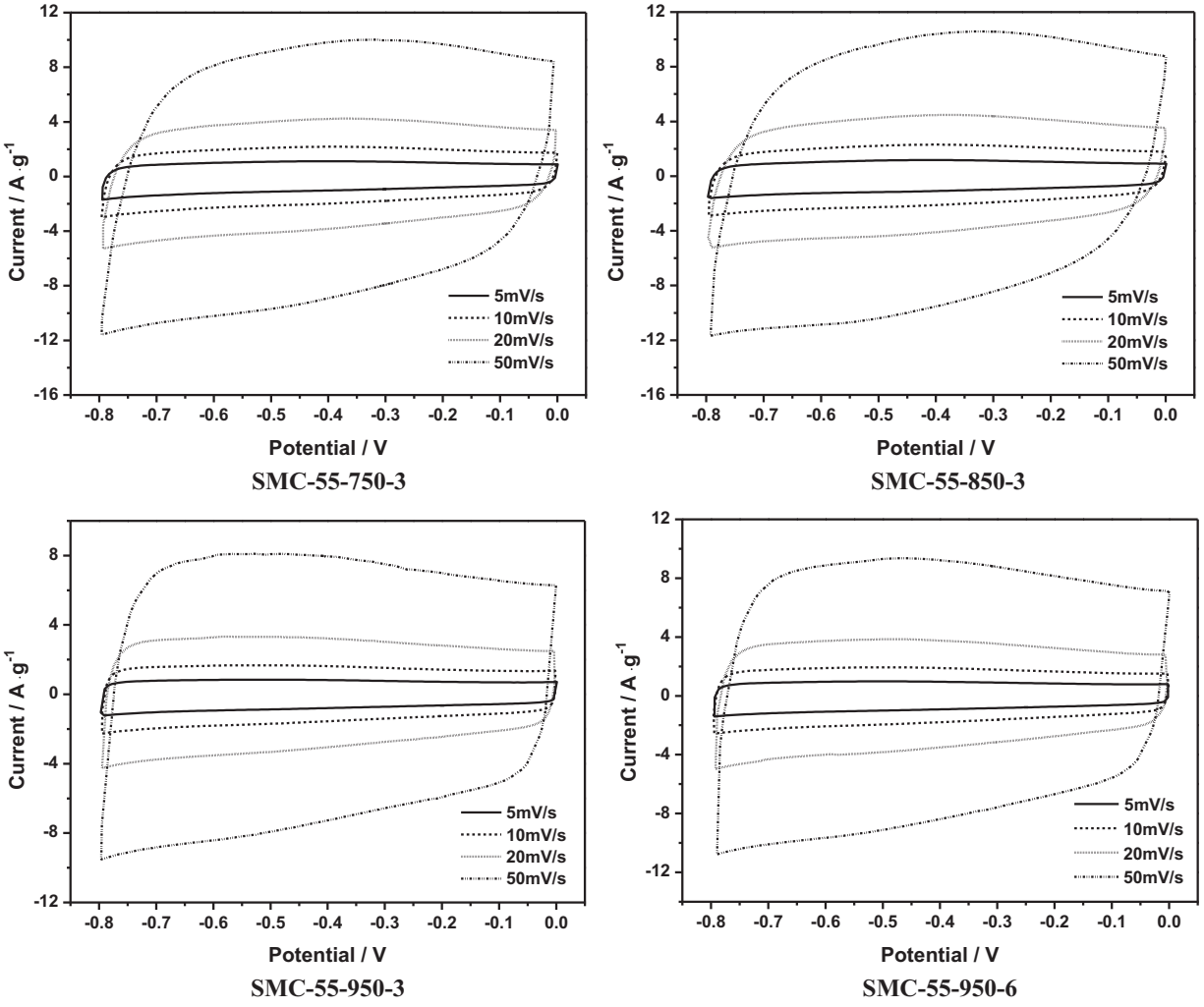

Fig. 6. Cyclic voltammograms at various scanning rates.

indicating growth of graphitic crystallite. In contrast, there is not any marked (0 0 2) diffraction peak for the carbons from pure starch, even through heat treatment at 950 °C for 6 h. This suggests that the graphitic structures were formed because of the effect of the needle-like template. However, different from transition metals particles [25,26], $Mg(OH)_2$ (or MgO) has no catalytic graphitization action. Besides, no (0 0 2) diffraction peak is observed for porous carbon obtained from the mixture of soluble starch and Mg acetate in a ratio of 5:5, which forms sphere-like nano-sized MgO about 10 nm after pyrolysis [18]. Therefore, it may be presumed that the special one dimensional morphology of templates caused a graphitization effect. Nevertheless, the (0 0 2) peaks are not so strong, and a turbostratic graphite structure is observed from HRTEM (Fig. 1c) observation, while some graphite lattice fringes which are not so regular can also be observed very near the pore walls, suggesting that the graphitization structures should be in partial and not perfect, or graphite-like structure.

When carbonized without any template, graphite crystallites from the pyrolysis of the starch were stacked disorderedly (Fig. 5a). In the presence of needle-like nano-sized $Mg(OH)_2$ (or MgO), the one dimensional nano-sized particles acted as director reagent during the pyrolysis of the starch, different from catalytic graphitization mechanism of transition metal particles, such as Fe and Ni [26,27]. The graphite crystallites tightly closed to the one dimensional templates were stacked orderedly along the axial direction of the templates, while those crystallites far from the templates were stacked disorderedly (Fig. 5b). Thus, the graphite-like structure in partial region was formed, but the disorderedly stacked crystallites were dominating in the porous carbon. Increasing the treatment temperature or the duration, the orientation degree of those 'ordered stacked' graphite crystallites was improved. Even though graphitization was improved in limited region, it was favorable to increase the carbon's electrical conductivity due to orientation of the carbon layers [28].

3.2. Electrochemical characterization

Fig. 6 shows cyclic voltammogramms at various scan rates from 5 mV s^{-1} to 50 mV s^{-1} at the potential range of −0.8 V to 0 V (vs. Hg/HgO) for porous carbons. All the samples exhibit typical quasi-rectangular curve shapes at low scan rate of 5 mV s^{-1}. With increasing scan rates, rectangular curve shapes of samples treated at high temperature (SMC-55-950-3 and SMC-55-950-6) are kept well, while the curve shape of SMC-55-750-3 and SMC-55-850-3, which treated at lower temperature, show distortion to some extent. The voltammogram shape is affected by the RC time constant (τ) of the electrode. A higher value of τ results in a longer transient part (less steepness in the current change of CV curve at the switching potential), which means worse collapse of the rectangular shape [29]. The nearly 90° change in the CV curves of at the switching potential suggests that samples treated at high temperature have small

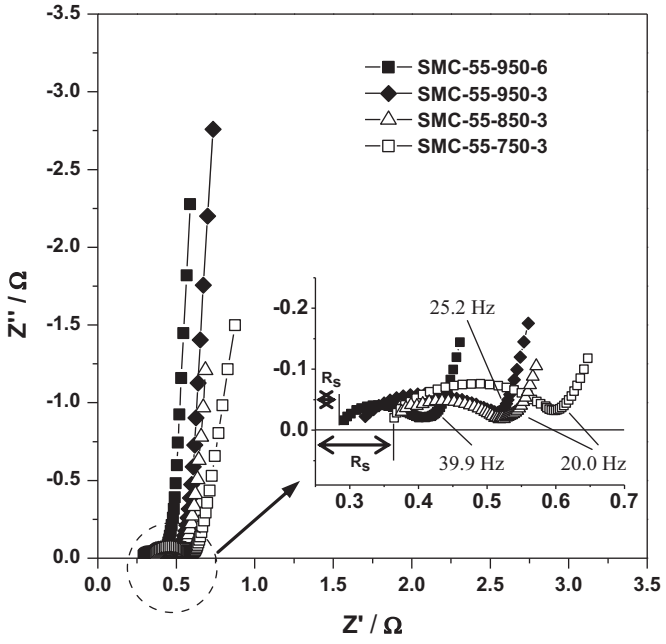

Fig. 7. Nyquist plots at AC frequency ranging from 20 kHz to 0.1 Hz.

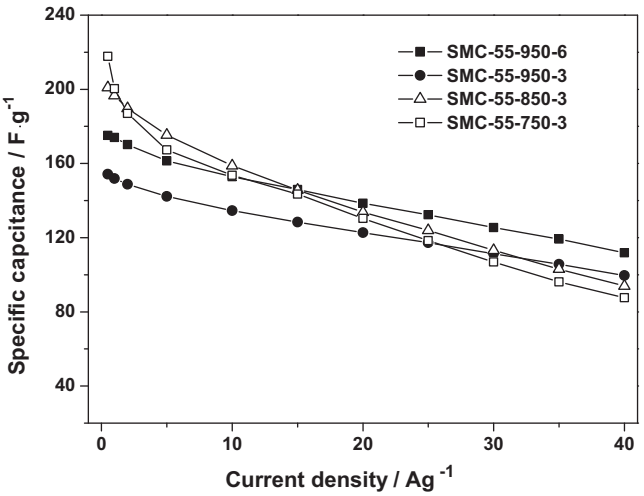

Fig. 8. Capacitances of galvanostatic charge/discharge at different currents.

time constants as an ideal capacitor, which indicate the excellent capacitive ability of even at high current density.

Fig. 7 illustrates the electrochemical impedance spectra of the carbon samples. In the Nyquist plots, a depressed semicircle is observed at the region from high to middle frequency, which may be ascribed to the charge transfer processes at the carbon electrode surface [3,30]. The typical characteristic of activated carbon electrochemical capacitor with a 45° Warburg line in the middle frequency range [3,31], so-called finite length capacitive effects plots that corresponds to the ions diffusion in a porous electrode, is not observed. This suggests that electrolyte ions transfer in the straight tunnel-like pores of the resultant mesoporous carbons is so rapid as to ignore the finite length capacitive influence nearly. As frequency decreased, the plot transits the semicircle to a closely vertical line parallel to the imaginary axis, which is characteristic of capacitive behavior. The crossing of this semicircle (or 45° Warburg line in other typical porous electrode) with the vertical line defines the "knee frequency" or "transition frequency". The higher value of the frequency is, the easier the accessibility of hydrated ions into the pores [31,32]. The knee frequencies of the resultant samples reach a level of tens Hz, which is one order of magnitude higher than that of activated carbons [31], and similar to that of order mesoporous carbons [33]. According to transmission line model for impedance spectrum, the knee frequency is influenced by depth and diameter of the pore in electrode material [34]. The dominant mesopores in the resultant porous carbon lead to a lower solution resistance in the pores, while one dimension morphology of straight tunnel-like pore structure is also favorable for hydrated ions to transfer and access into the pores interior. Consequently, the transition frequency shifts to high frequency side as comparing with conventional activated carbons, which usually possess dominant micropores and ramiform pore structures. The sum of the resistance of the electrolyte solution, the intrinsic resistance of the active material, and the contact resistance of the interface active material/current collector, R_s, can be obtained from the intercept of the semicircle in the high frequency region with the real axis. It can be seen from Fig. 8 that, R_s decreases with increase in temperature and duration. In our experiment, the contact resistances and the electrolyte resistances were nearly identical in all samples, so the decrease of R_s indicates a decrease of the carbon resistance, or increase of the electrical conductivity, corresponding to the XRD results.

Fig. 8 shows the capacitances of the resultant mesoporous carbons obtained from galvanostatic charge/discharge at different currents. The specific capacitance – C_s ($F g^{-1}$) is calculated from the discharge process on the basis of equation: $C_s = I\Delta t/(\Delta V \cdot m)$, where I is the current loaded, Δt is the discharge time, ΔV is the potential change during the discharge process, and m is the mass of porous carbon in the test electrode. At low charge–discharge current density of 0.5 $A g^{-1}$, SMC-55-750-3, the sample treated at relatively lower temperature, exhibits a capacitance of as high as 217 $F g^{-1}$, namely 21.4 $\mu F cm^{-2}$ (expressed per unit of BET surface area), which is higher than that of ordered mesoporous carbons with similar specific surface areas and pore sizes [2,33,35]. However, the capacitances of samples decrease with increasing treating temperature. The capacitance of SMC-55-850-3 is 201 $F g^{-1}$, and SMC-55-950-3 only reaches a capacitance of 154 $F g^{-1}$, namely 12.1 $\mu F cm^{-2}$. Generally, the capacitance is contributed by the large surface of porous carbon where electric double layers are formed. Besides, the varieties in the pores morphology and varieties in surface chemistry (e.g., wettability and pseudocapacitive contributions) are also two major factors that contribute to the overall capacitance [36]. For the present samples, the surface areas and pore morphologies are similar. Whereas, the sample obtained at lower temperature would remain more functional groups on the pore surfaces [37,38], which may resulted in better wettability, corresponding to a higher capacitance. The functional groups may also contribute some Faradic pseudo capacitance to the total capacitance. When increasing heat treatment temperature, the wettability of pore surfaces was degraded. While the orientation degree of those 'ordered stacked' graphite crystallites in partial region was improved, as mentioned above. As a result, the basal layer amount would increased, which capacitance was reported to be an order of magnitude smaller than that of the edge orientation of graphite [36]. Thus, the capacitances decreased with increasing treatment temperature.

It should be noted that, increasing the heating duration at 950 °C, SMC-55-950-6 shows an increased capacitance of 175 $F g^{-1}$ (namely 16.6 $\mu F cm^{-2}$) at 0.5 $A g^{-1}$, 13.6% higher than that of SMC-55-950-3. As showed by nitrogen adsorption, SMC-55-950-6 possesses a similar specific surface as SMC-55-950-3, but a larger pore size and a larger total pore volume in comparison to SMC-55-950-3. While the samples in the present work possess straight tunnel-like porous structure derived from one dimensional template, approaching the cylindrical pores. According to 'EDCCs'

(electric double-cylinder capacitors) model [5,39], for micropores and mesoporous carbon materials, it seems reasonable to include the influence of pore curvature to describe the capacitance expressed per unit of BET area. Solvated counterions enter the cylindrical mesopores and approach the pore walls to form EDCCs, and the normalized capacitance will increase with pore size at the mesopores region, especially for mesopores small than 20 nm. Here the results verified 'EDCCs' theoretical model for nanoporous carbon ECs.

The charge/discharge performance at high rate can estimate the capacitive properties, the higher the capacitance retention at high rate, the better capacitive performance. From Fig. 8, it can be seen that with increasing charge–discharge current densities, the capacitance of porous carbon treated at 750 °C decreases rapidly. At 40 A g^{-1}, 40% capacitance is retained only. For samples treated for different durations at higher temperature (950 °C), the falling tendency of the capacitance is similar as the applied current increased, and excellent capacitance retainment is exhibited at high current densities. SMC-55-950-6 retained 72% capacitance up to a current of 40 A g^{-1}. It indicates that such kind of mesoporous carbon presents superior rate capability, in agreement with the results of CV and EIS test.

4. Conclusions

An extraordinary mesoporous carbon with good electrochemical performance was prepared from a mixture of the soluble starch with needle-like nano-sized $Mg(OH)_2$ particles. The as-prepared mesoporous carbons exhibited straight tunnel-like pore structure that resembled the shape of the template, and possessed high surface areas of more than 1000 m^2 g^{-1} and large pore volumes. The special one dimensional morphology of templates caused a graphitization effect, different from catalytic graphitization mechanism of transition metal particles. In a 6 M KOH aqueous electrolyte, a high knee frequency of tens Hz was detected. Such kind of mesoporous carbons exhibited high capacity and excellent power performance. Besides, porous carbons obtained through this route will also be promising electrode materials for fuel cells application because of their disordered pore structures [40] and large pore volumes.

Acknowledgements

The authors gratefully thank the National Natural Science Foundation of China (Grant Nos. 50972064, 50972065 and 50632040) and the Program for New Century Excellent Talents in University (NCET-10-0496) for financial supports.

References

[1] K.W. Nam, K.B. Kim, J. Electrochem. Soc. 153 (2006) A81–A88.
[2] A.B. Fuertes, G. Lota, T.A. Centeno, E. Frackowiak, Electrochim. Acta 50 (2005) 2799–2805.
[3] B.E. Conway, Electrochemical Supercapacitors: Scientific Fundamentals, Technological Applications, Kluwer Academic/Plenum Publishers, New York, 1999.
[4] J. Chmiola, G. Yushin, Y. Gogotsi, C. Portet, P. Simon, P.L. Taberna, Science 313 (2006) 1760–1763.
[5] J.S. Huang, B.G. Sumpter, V. Meunier, Chem. Eur. J. 14 (2008) 6614–6626.
[6] H. Itai, H. Nishihara, T. Kogure, T. Kyotani, J. Am. Chem. Soc. 133 (2011) 1165–1167.
[7] A. Stein, Z.Y. Wang, M.A. Fierke, Adv. Mater. 21 (2009) 265–293.
[8] J. Lee, J. Kim, T. Hyeon, Adv. Mater. 18 (2006) 2073–2094.
[9] Y.D. Xia, Z.X. Yang, R. Mokaya, Nanoscale 2 (2010) 639–659.
[10] C.D. Liang, Z.J. Li, S. Dai, Angew. Chem. Int. Ed. 47 (2008) 3696–3717.
[11] C.D. Liang, K.L. Hong, G.A. Guiochon, J.W. Mays, S. Dai, Angew. Chem. Int. Ed. 43 (2004) 5785–5789.
[12] S. Tanaka, N. Nishiyama, Y. Egashira, K. Ueyama, Chem. Commun. (2005) 2125–2127.
[13] F.Q. Zhang, Y. Meng, D. Gu, Y. Yan, C.Z. Yu, B. Tu, D.Y. Zhao, J. Am. Chem. Soc. 127 (2005) 13508–13509.
[14] Y. Meng, D. Gu, F.Q. Zhang, Y.F. Shi, L. Cheng, D. Feng, Z.X. Wu, Z.X. Chen, Y. Wan, A. Stein, D.Y. Zhao, Chem. Mater. 18 (2006) 4447–4464.
[15] C.D. Liang, S. Dai, J. Am. Chem. Soc. 128 (2006) 5316–5317.
[16] Y. Huang, H.Q. Cai, T. Yu, F.Q. Zhang, F. Zhang, Y. Meng, D. Gu, Y. Wan, X.L. Sun, B. Tu, D.Y. Zhao, Angew. Chem. Int. Ed. 46 (2007) 1089–1093.
[17] Y.H. Deng, T. Yu, Y. Wan, Y.F. Shi, Y. Meng, D. Gu, L.J. Zhang, Y. Huang, C. Liu, X.J. Wu, D.Y. Zhao, J. Am. Chem. Soc. 129 (2007) 1690–1697.
[18] T. Morishita, Y. Soneda, T. Tsumura, M. Inagaki, Carbon 44 (2006) 2360–2367.
[19] T. Morishita, K. Ishihara, M. Kato, M. Inagaki, Carbon 45 (2007) 209–211.
[20] M. Inagaki, S. Kobayashi, F. Kojin, N. Tanaka, T. Morishita, B. Tryba, Carbon 42 (2004) 3153–3158.
[21] J.A. Fernández, T. Morishita, M. Toyoda, M. Inagaki, F. Stoeckli, T.A. Centeno, J. Power Sources 175 (2008) 675–679.
[22] L.Z. Qiu, R.C. Xie, P. Ding, B.J. Qu, Compos. Struct. 62 (2003) 391–395.
[23] Y. Ding, G.T. Zhang, H. Wu, B. Hai, L.B. Wang, Y.T. Qian, Chem. Mater. 13 (2001) 435–440.
[24] M. Kruk, M. Jaroniec, Chem. Mater. 13 (2001) 3169–3183.
[25] F.J. Maldonado-Hodar, C. Moreno-Castilla, J. Rivera-Utrilla, Y. Hanzawa, Y. Yamada, Langmuir 16 (2000) 4367–4373.
[26] M. Inagaki, Y. Okada, V. Vignal, H. Konno, K. Oshida, Carbon 36 (1998) 1706–1708.
[27] M. Sevilla, A.B. Fuertes, Carbon 44 (2006) 468–474.
[28] A.G. Pandolfo, A.F. Hollenkamp, J. Power Sources 157 (2006) 11–27.
[29] H.Q. Li, Y.G. Wang, C.X. Wang, Y.Y. Xia, J. Power Sources 185 (2008) 1557–1562.
[30] K. Tõnurist, A. Jänes, T. Thomberg, H. Kurig, E. Lust, J. Electrochem. Soc. 156 (2009) A334–A342.
[31] Q.Y. Li, H.Q. Wang, Q.F. Dai, J.H. Yang, Y.L. Zhong, Solid State Ionics 179 (2008) 269–273.
[32] P.L. Taberna, P. Simon, J.F. Fauvarque, J. Electrochem. Soc. 150 (2003) A292–A300.
[33] H.Q. Li, J.Y. Luo, X.F. Zhou, C.Z. Yu, Y.Y. Xia, J. Electrochem. Soc. 154 (2007) A731–A736.
[34] M. Itagaki, S. Suzuki, I. Shitanda, K. Watanabe, H. Nakazawa, J. Power Sources 164 (2007) 415–424.
[35] M. Sevilla, S. Alvarez, A.B. Fuertes, Microporous Mesoporous Mater. 74 (2004) 49–58.
[36] D.Y. Qu, J. Power Sources 109 (2002) 403–411.
[37] A. Yoshida, I. Tanahashi, A. Nishino, Carbon 28 (1990) 611–615.
[38] V. Ruiz, C. Blanco, E. Raymundo-Pinero, V. Khomenko, F. Beguin, R. Santamaria, Electrochim. Acta 52 (2007) 4969–4973.
[39] J.S. Huang, B.G. Sumpter, V. Meunier, Angew. Chem. Int. Ed. 47 (2008) 520–524.
[40] D.R. Rolison, Science 299 (2003) 1698–1701.